applied sciences

MDPI

Article

Effect Range of the Material Constraint in Different Strength Mismatched Laboratory Specimens

Yue Dai [1], Jie Yang [1,*] and Haofeng Chen [2]

[1] Shanghai Key Laboratory of Multiphase Flow and Heat Transfer in Power Engineering, School of Energy and Power Engineering, University of Shanghai for Science and Technology, Shanghai 200093, China; daiyue9611@sina.com

[2] Department of Mechanical & Aerospace Engineering, University of Strathclyde, Glasgow G1 1XJ, UK; haofeng.chen@strath.ac.uk

* Correspondence: yangjie@usst.edu.cn; Tel.: +86-021-5527-2320

Received: 22 March 2020; Accepted: 31 March 2020; Published: 2 April 2020

Abstract: Different strength mismatched laboratory specimens that contain the compact tension (CT), single edge-notched tensile (SENT), and central-cracked tension (CCT) specimens with various specimen geometries, loading configurations, and initial cracks were selected to investigate the effect range of the material constraint systematically. The results showed that the effect range of material constraint exists in all the strength mismatched specimens and structures. The numerical value of the effect range is influenced by the geometry constraint. The high geometry constraint reduces the effect range of material constraint. When a material is located outside the effect range of material constraint, the fracture resistance curves and crack propagation paths of the specimens and structures are no longer influenced by the mechanical properties of the material. In addition, an interaction exists between the geometry constraint and material constraint. The high geometry constraint strengthens the effect of material constraint, whereas the fracture resistance curve and crack propagation path are insensitive to the material constraint under the low geometry constraint. The results in this study may provide scientific support for the structure integrity assessment and the design of strength mismatched structures.

Keywords: material constraint; effect range; different laboratory specimens; fracture resistance curve; crack propagation path; structural integrity

1. Introduction

Constraint is the resistance of a specimen or structure against plastic deformation. It contains geometry constraint and material constraint. The geometry constraint is affected by the dimension of specimen, whereas the material constraint is affected by the strength mismatch between different materials. Both of them can affect the fracture behavior of the material significantly.

The material constraint was first proposed by Joch et al. [1] and Burstow et al. [2] to show the changing of slip-line fields with the yield strength of the base material. Then, some parameters were established to characterize the material constraint. Zhang et al. [3] established a material constraint parameter M to investigate the two-material problem where the crack was located in the interface of two dissimilar materials. Betegón et al. [4] defined another material constraint parameter β_m which suited the overmatched welded joints. Yang et al. [5–7] proposed a unified constraint parameter A_p which can characterize both material constraint and geometry constraint.

In addition, the fracture resistance curve, crack propagation path, fracture toughness, crack-tip fields of the strength mismatched structures, especially in welded joint, affected by the material constraint were also investigated widely.

Wang et al. [8,9] and Sarikka et al. [10] investigated the fracture resistance curve of dissimilar metal welded joint (DMWJ) influenced by material constraint. Fan et al. [11–13] studied the fracture resistance curve of bi-material welded joint influenced by material constraint. Samal et al. [14] and Yang et al. [15] studied the deviation of crack propagation path in DMWJ influenced by material constraint. Lindqvist et al. [16] and Jang et al. [17] focused on their studies on the fracture toughness of DMWJ affected by material constraint. Xue et al. [18] and Zhu et al. [19] studied the crack-tip fields of DMWJ influenced by material constraint. Younise et al. [20] and Xue et al. [21] studied the crack-tip fields of welded joint affected by material heterogeneity. Khan et al. [22,23] studied the structure of stress fields for stationary crack in welded joint influenced by material constraint.

Nevertheless, most studies above focused their attention on the strength mismatch of both sides of the crack, such as over-match and under-match. There is another interesting issue, the effect range of the material constraint, which also needs to be clarified. This includes whether exists an effect range of material constraint or not, who effects it, and whether the fracture resistance and crack propagation path are affected by the material which is located outside the effect range or not.

In the previous studies [24,25], the effect range of the material constraint has been studied and verified in the single-edge-notched bend (SENB) specimen. However, it is not enough to arrive at a conclusion that the effect range of material constraint exists in all the structures with different geometries and loading configurations. Thus, in this study, more laboratory specimens which contain the compact tension (CT), single edge-notched tensile (SENT), and central-cracked tension (CCT) specimens with various specimen geometries, loading configurations, and initial cracks were selected to further study the effect range of the material constraint.

2. Different Strength Mismatched Laboratory Specimens

2.1. Materials

To make the laboratory specimens reflect the actual situation of the structures, the materials used in this study were selected from an actual DMWJ that was used in the nuclear power plants for connecting the pipe-nozzle and safe end, as shown in the Figure 1.

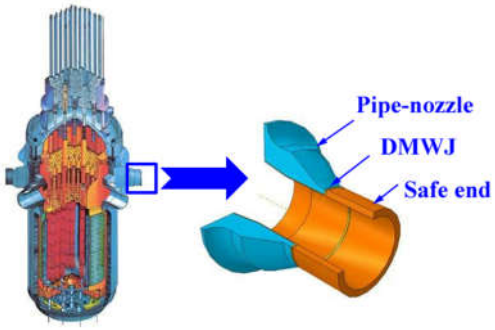

Figure 1. Connection diagram of the dissimilar metal welded joint (DMWJ) with pipe-nozzle and safe end.

The structure of the DMWJ is shown in the Figure 2(a) [26]. There are four materials in this DMWJ: the ferrite low-alloy steel A508, the buttering material 52 Mb, the weld material 52 Mw, and the austenitic stainless steel 316 L. The true stress–strain curves of the four materials are shown in Figure 2(b) [8].

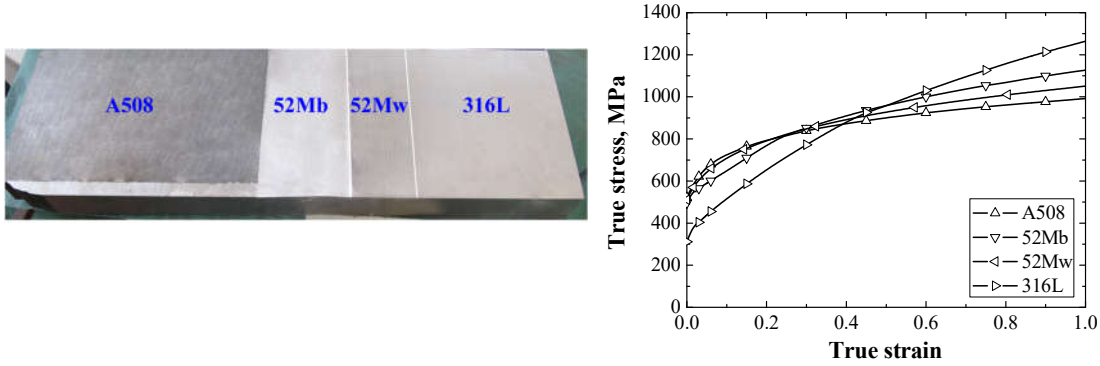

Figure 2. The structure of the DMWJ [26] (**a**) and the true stress-strain curves of the four materials in the DMWJ [8] (**b**).

2.2. The Design of Different Strength Mismatched Laboratory Specimens

Three sets of strength mismatched laboratory specimens (CT, SENT, and CCT specimens) with various specimen geometries, loading configurations, and initial cracks were selected in this study, as shown in the Figure 3. The SENB specimen has been investigated in the previous studies of authors [24,25].

Each set of specimen contains two kinds of specimens, which can be called as the "121" specimen and "1231" specimen. The structures of these specimens are similar to hamburgers, as shown in the Figure 3. The "121" specimen indicates that the specimen contains "1" and "2" two kinds of materials, and the materials in the specimen from up to down are "1," "2," and "1". The "1231" specimen indicates that the specimen contains "1," "2," and "3" three kinds of materials, and the materials in the specimen from up to down are "1," "2," "3," and "1." For the "121" specimen, the initial crack is a center crack and located in the center of the "2"; for the "1231" specimen, the initial crack is an interface crack and located in the interface of the "2" and "3".

Not only that, two initial crack depths denoted as $a / W = 0.2$ (shallow crack) and $a / W = 0.5$ (deep crack) were also set for each specimen.

For all the "121" specimens, different material constraints were obtained by changing the width of material 52 Mb from 0 mm to 38.4 mm. When the width of material 52 Mb is 0 mm, the CT, SENT, and CCT specimens have homogeneous material A508; when the width of material 52 Mb is 38.4 mm, the CT, SENT, and CCT specimens have homogeneous material 52 Mb. For all the "1231" specimens, different material constraints were obtained by changing the widths of material 52 Mb and material 52 Mw from 0 mm to 19.2 mm simultaneously. When the widths of material 52 Mb and material 52 Mw are 0 mm, the CT, SENT, and CCT specimens have homogeneous material A508; when the widths of material 52 Mb and material 52 Mw are 19.2 mm, the CT, SENT, and CCT specimens have bimetallic material 52 Mb and 52 Mw.

A total of 72 models were included in this study.

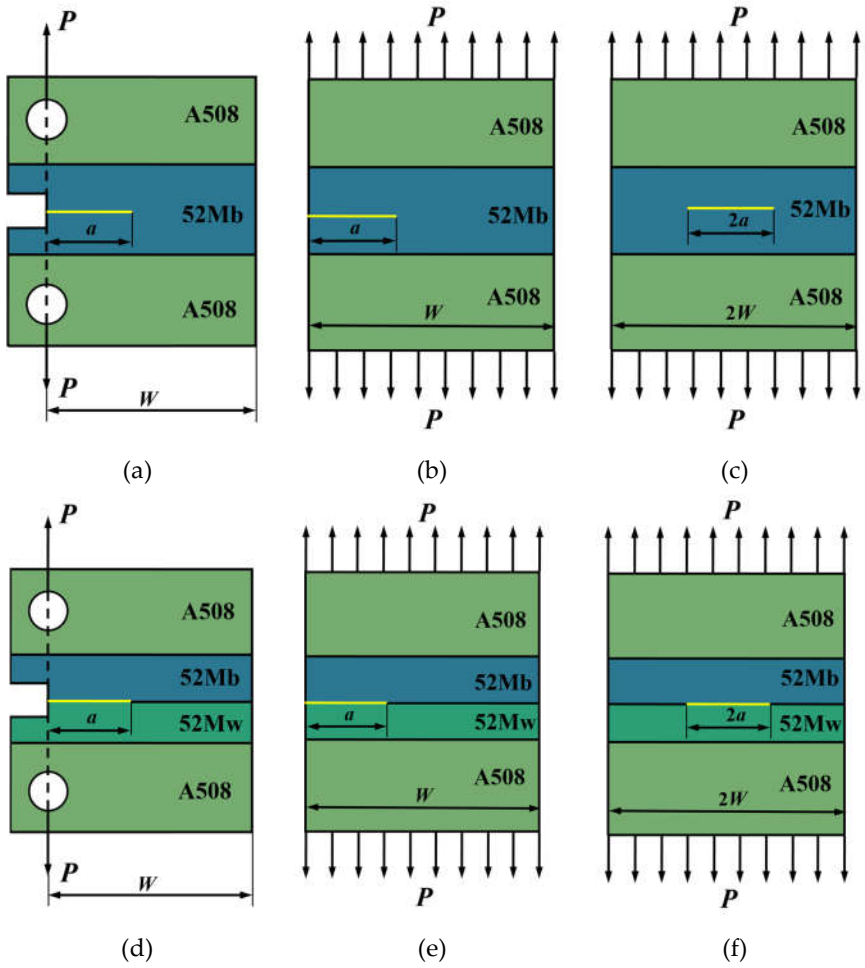

Figure 3. The geometries and loading configurations of different kinds of specimens, (**a**) CT-"121" specimen, (**b**) SENT-"121" specimen, (**c**) CCT-"121" specimen, (**d**) CT-"1231" specimen, (**e**) SENT-"1231" specimen, and (**f**) CCT-"1231" specimen.

2.3. GTN Damage Model

To obtain the fracture resistance curves and crack propagation paths of different strength mismatched laboratory specimens under various material constraints, the finite element method (FEM) simulation based on Gurson-Tvergaard-Needleman (GTN) damage model was used to simulate the progress of crack growth in the specimens. There are nine parameters in the GTN damage model, and these parameters of the four materials have been obtained and verified, as shown in Table 1 [27].

Table 1. The nine Gurson-Tvergaard-Needleman (GTN) damage parameters of the four materials in the DMWJ [27].

Material	q_1	q_2	q_3	ε_N	S_N	f_N	f_0	f_C	f_F
A508	1.5	1	2.25	0.3	0.1	0.002	0.00008	0.04	0.25
52Mb	1.5	variable	2.25	0.3	0.1	0.002	0.000001	0.04	0.25
52Mw	1.5	1	2.25	0.3	0.1	0.002	0.00015	0.04	0.25
316L	1.5	variable	2.25	0.3	0.1	0.002	0.000001	0.04	0.25

The GTN damage model has been implemented in the ABAQUS code. During the finite element analysis, the 4-node plane strain quadrilateral element with reduced integration (CPE4R) was used. The typical finite element meshes of the CT-"121" model with a / W = 0.5 is illustrated in the Figure 4(a). In the crack growth region, the minimum mesh size is 0.1 mm × 0.05 mm [28], as shown in the

Figure 4(b). The mesh sensitivity study has been done and the same mesh size was used in all the models. This typical model contains 25208 elements and 25730 nodes.

Based on the FEM simulation results, the fracture resistance curves and crack propagation paths of different strength mismatched laboratory specimens under various material constraints can be determined [6].

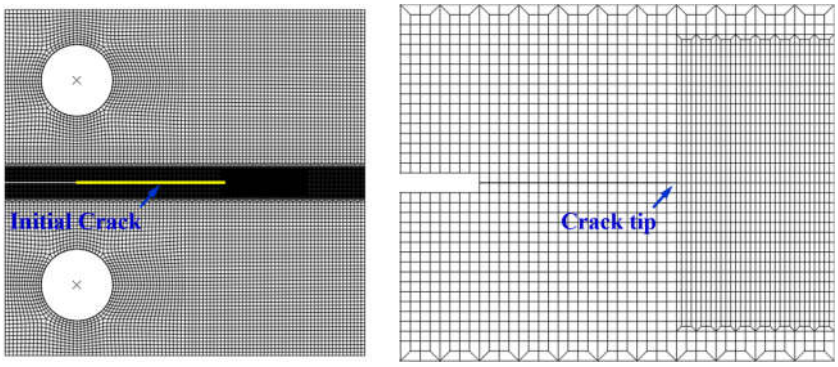

Figure 4. The typical finite element meshes of the CT-"121" model with a / W = 0.5 (**a**) and the local meshes in the crack growth region (**b**).

3. Results and Discussion

3.1. CT Specimen

3.1.1. Two kinds of CT specimens with shallow crack

Figure 5 presents the fracture resistance curves and crack propagation paths of the CT-"121" and CT-"1231" specimens with shallow crack under different material constraints. Figure 5(a) presents the fracture resistance curves of the CT-"121" specimens with shallow crack. The fracture resistance curves are related to the strengths of the materials A508 and 52 Mb. Because the strength of the material 52 Mb is higher than the material A508, the increasing of the width of material 52 Mb increases the fracture resistance of the specimen. The Figure 5(b) shows a same trend with Figure 5(a). Increasing the widths of material 52 Mb and material 52 Mw, which have higher strength, increase the fracture resistance of specimen.

However, the fracture resistance curves of the CT-"121" and CT-"1231" specimens with shallow crack have not reached a steady state with changing of the widths of material 52 Mb and material 52 Mw, hence we cannot arrive at a conclusion whether the effect range of material constraint exists or not in the CT specimen.

In addition, Figure 5(c) presents that all the cracks propagate straight and have not changed considerably under different material constraints in the CT-"121" specimens with shallow crack. It is because that the initial crack in this kind of specimen is a center crack and located in the center of the material 52 Mb, the strengths of materials at the both sides of the crack are symmetric. This is different from the CT-"1231" specimens with shallow crack. In the CT-"1231" specimens, the initial crack is an interface crack and located in the interface of the material 52 Mb and material 52 Mw. The crack propagation paths deviate to the side of material 52 Mw, which has a lower strength than material 52 Mb in the process of crack growth, as shown in the Figure 5(d). By increasing the widths of material 52 Mb and material 52 Mw, the deviation becomes more obvious accompanied by the increasing of strength mismatch.

Similarly, with the fracture resistance curves, the crack propagation paths of the CT-"121" and CT-"1231" specimens with shallow crack have not reached a steady state with changing of the widths of material 52 Mb and material 52 Mw. It is impossible to arrive at a conclusion whether the effect range of material constraint exists or not in the CT specimen only, as shown in Figure 5.

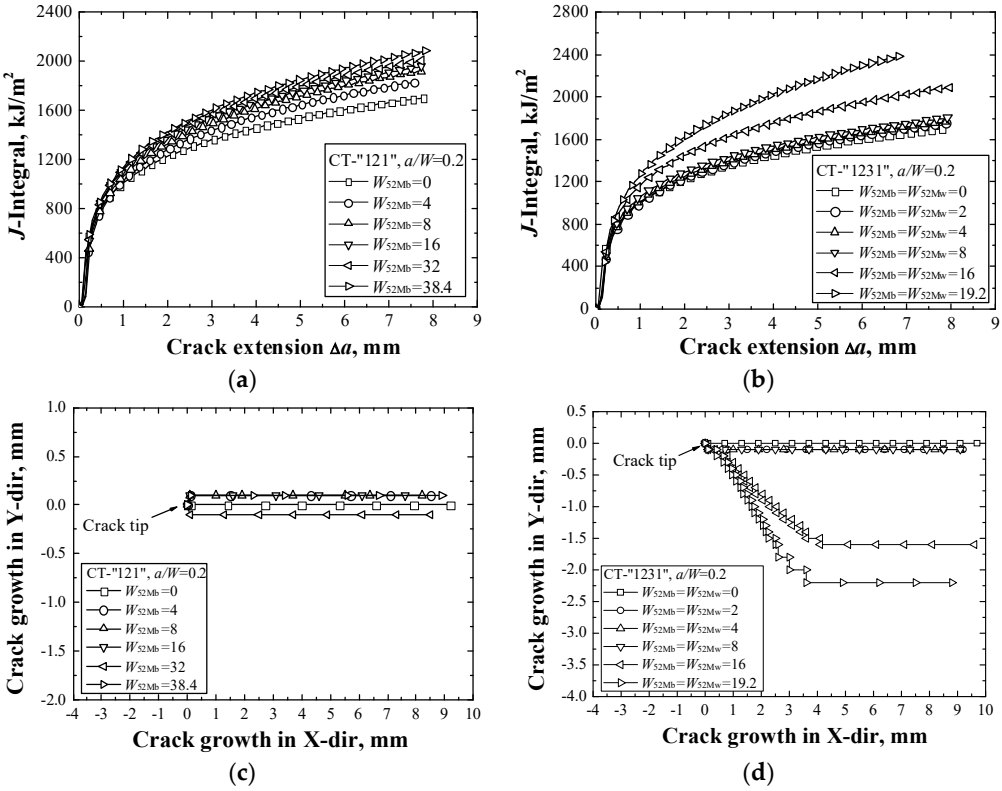

Figure 5. The fracture resistance curves of CT-"121" (**a**) and CT-"1231" (**b**) specimens with shallow crack together with the crack propagation paths of CT-"121" (**c**) and CT-"1231" (**d**) specimens with shallow crack.

3.1.2. Two Kinds of CT Specimens with Deep Crack

Figure 6 presents the fracture resistance curves and crack propagation paths of the CT-"121" and CT- "1231" specimens with deep crack under different material constraints. Figure 6(a) presents the fracture resistance curves of the CT-"121" specimens with deep crack.

It is different with the CT-"121" specimens with shallow crack in the Figure 5(a). First, the fracture resistance curves have an obvious steady state when the width of the material 52 Mb reaches 16 mm. When the width of the material 52 Mb is longer than 16 mm, the fracture resistance curves of the CT-"121" specimens with deep crack no longer change. It means that an effect range of the material constraint exists in the CT-"121" specimen with deep crack. When the width of the material 52 Mb is longer than 16 mm, it exceeds the effect range of the material constraint. Second, the fracture resistance curves decrease first when the width of the material 52 Mb changes from 0 mm to 4 mm. This is the same for the SENB-"1231" specimen in the previous study of the authors [23]. The decreasing of the fracture resistance curves is related to the high geometry constraints of CT and SENB specimens with deep crack. There exists interaction between geometry constraint and material constraint. The high geometry constraints in the CT and SENB specimens with deep crack strengthen the effect of material constraint and decrease the fracture resistance curve first. When the width of the material 52 Mb is longer than 4 mm, the overall strength and fracture resistance curve of the CT-"121" specimen with deep crack increase.

Figure 6(b) presents the fracture resistance curves of the CT-"1231" specimens with deep crack. Similarly, with the CT-"121" specimen with deep crack in the Figure 6(a), an effect range of the material constraint also exists in the CT-"1231" specimen with deep crack.

Figure 6(c) and (d) present the crack propagation paths of the CT-"121" and "1231" specimens with deep crack. Figure 6(c) presents that all the cracks propagate straight and have not changed considerably under different material constraints in the CT-"121" specimens with deep crack. It is

also because that the initial crack located in the center of the material 52 Mb, the strengths of materials at the both sides of the crack are symmetric. Figure 6(d) presents that the crack propagation paths deviate to the side of material 52 Mw which has a lower strength than material 52 Mb in the process of crack growth. With an increase in the widths of material 52 Mb and material 52 Mw, the deviation becomes more obvious first then remains steady. It is consistent with the fracture resistance curves in the Figure 6(b), and means that the effect range of the material constraint exists in the CT-"1231" specimen with deep crack. When the total width of the material 52 Mb and material 52 Mw is longer than 16 mm, it exceeds the effect range of the material constraint, and the crack propagation paths no longer change.

Considering both Figure 5 and Figure 6, it can be concluded that the effect range of material constraint exists in the CT specimen. Not only that, the effect range is influenced by the geometry constraint induced by the crack depth. The high geometry constraint (deep crack) against the plastic deformation at crack tip and reduces the effect range of material constraint. For the CT specimen with shallow crack and low geometry constraint, the effect range is greater than 38.4 mm, and thus the steady state has not been obtained in the Figure 5.

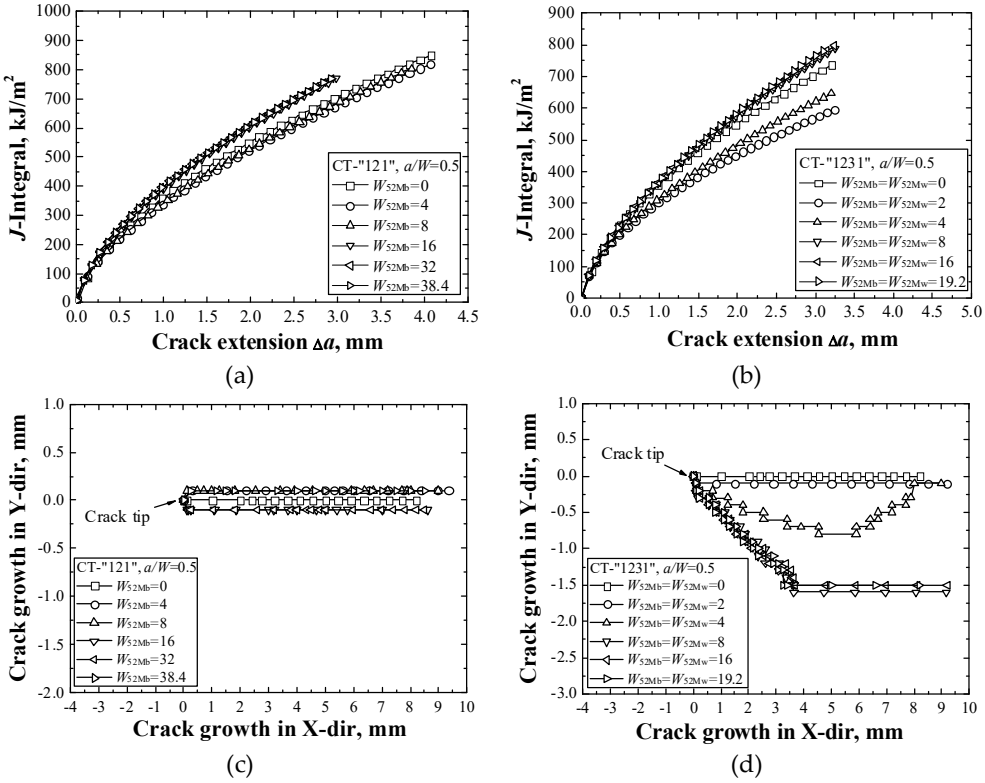

Figure 6. The fracture resistance curves of CT-"121" (**a**) and CT-"1231" (**b**) specimens with deep crack together with the crack propagation paths of CT-"121" (**c**) and CT-"1231" (**d**) specimens with deep crack.

3.2. SENT Specimen

3.2.1. Two Kinds of SENT Specimens with Shallow Crack

Figure 7 presents the fracture resistance curves and crack propagation paths of the SENT-"121" and SENT-"1231" specimens with shallow crack under different material constraints. Figure 7(a) and (b) presents that the fracture resistance curves of the SENT-"121" specimen and SENT-"1231" specimen show the same trends. It is related to the strengths of the materials A508, 52 Mb, and 52 Mw. Because the strengths of the materials 52 Mb and 52 Mw are higher than the material A508, the increasing of the widths of materials 52 Mb and 52 Mw increase the fracture resistances of specimens.

In addition, it can be also found that for both SENT-"121" and SENT-"1231" specimens, an obvious steady state exists in the fracture resistance curves. It means that the effect range of material constraint exists in the SENT-"121" and SENT-"1231" specimens with shallow crack.

Figure 7(c) presents that all the cracks propagate straight and have not changed considerably under different material constraints in the SENT-"121" specimens with shallow crack. It is because that the initial crack in this kind of specimen is a center crack and located in the center of the material 52 Mb, the strengths of materials at the both sides of the crack are symmetric. For the SENT-"1231" specimen with shallow crack, Figure 7(d) presents that the cracks also propagate straight and the crack propagation paths under different material constraints are similar. The similar crack propagation paths may be caused by the low geometry constraints of the SENT-"1231" specimens with shallow crack. Under the low geometry constraint, the crack propagation path is insensitive to the changing of material constraint.

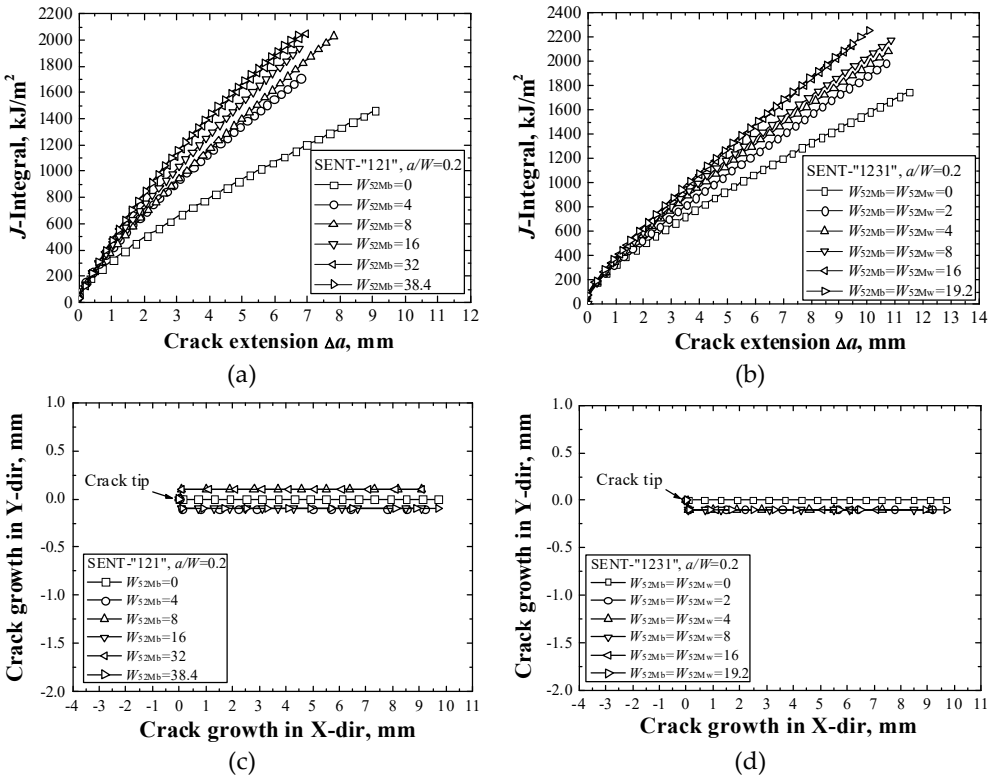

Figure 7. The fracture resistance curves of SENT-"121" (**a**) and SENT-"1231" (**b**) specimens with shallow crack together with the crack propagation paths of SENT-"121" (**c**) and SENT-"1231" (**d**) specimens with shallow crack.

3.2.2. Two Kinds of SENT Specimens with Deep Crack

Figure 8 presents the fracture resistance curves and crack propagation paths of the SENT-"121" and SENT-"1231" specimens with deep crack under different material constraints. Figure 8(a) presents the fracture resistance curves of the SENT-"121" specimens with deep crack. The fracture resistance curves are related to the strengths of the materials A508 and 52 Mb. Because the strength of the material 52 Mb is higher than the material A508, the increasing of the width of material 52 Mb increases the fracture resistance of the specimen. When the width of material 52 Mb reaches 32 mm, it exceeds the effect range of material constraint, and the fracture resistance curves of the SENT-"121" specimens with deep crack no longer change.

Different from the Figure 8(a), Figure 8(b) presents that the fracture resistance curves of the SENT-"1231" specimens with deep crack decrease first then increase, and finally remain steady with

increasing of the widths of material 52 Mb and material 52 Mw. Similarly, with CT-"121" and CT-"1231" specimens with deep crack in the Figure 6(a) and (b), the decreasing of the fracture resistance curves is also related to the high geometry and material constraints of the SENT-"1231" specimen with deep crack. The high constraint decreases the fracture resistance curve first. When the widths of the materials 52 Mb and 52 Mw are longer than 8 mm, the overall strength and fracture resistance curve of the SENT-"1231" specimen with deep crack increase. Because the material constraint of the SENT-"121" specimen is lower than SENT-"1231" specimen, the fracture resistance curves of the SENT-"121" specimens in Figure 8(a) have not decreased.

Figure 8(c) presents that all the cracks propagate straight and have not changed considerably under different material constraints in the SENT-"121" specimens with deep crack. Similarly, with SENT-"121" specimens with shallow crack, it is also because the strengths of materials at the both sides of the crack are symmetric.

For the SENT-"1231" specimen with deep crack, Figure 8(d) presents that the crack propagation paths deviate to the side of the material 52 Mb which has a higher strength than material 52 Mw in the process of crack growth. It is different with the CT specimens in this study and the SENB specimens in the previous studies [24,25], and may be related to the loading configuration. The crack bears the bending stress in the CT and SENB specimens, but bears the shearing stress in the SENT specimen. The crack propagation path deviates to the side of high strength under the shearing stress in the SENT specimen.

Taking into account both Figures 7 and 8, we can arrive to a conclusion that the effect range of material constraint also exists in the SENT specimen.

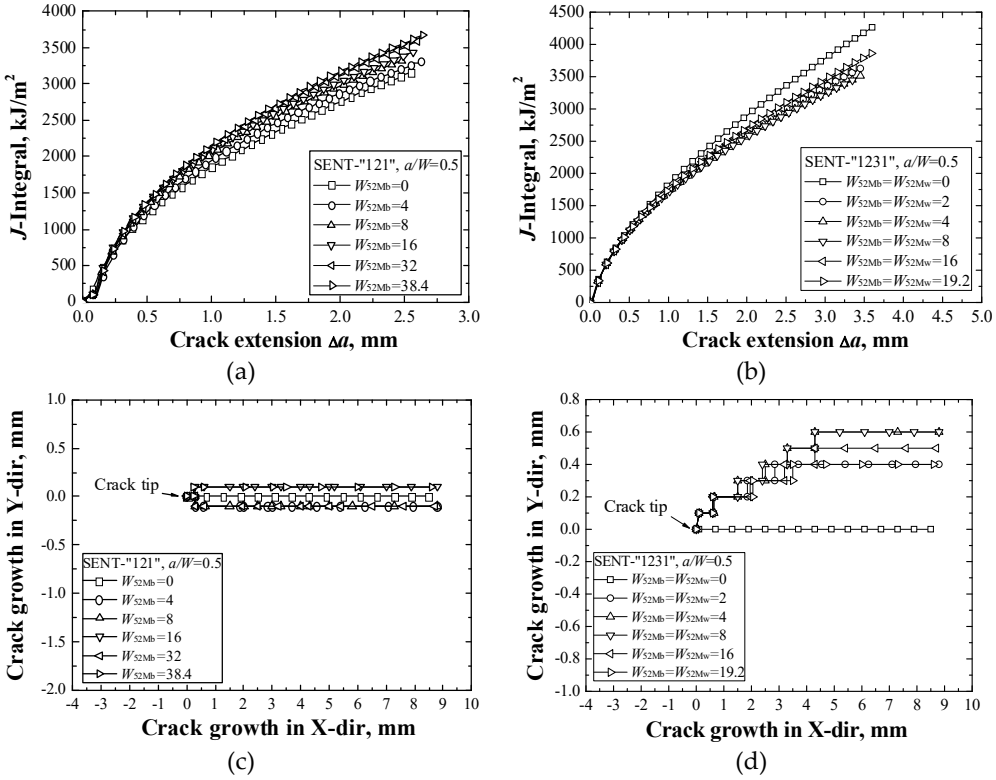

Figure 8. The fracture resistance curves of SENT-"121" (**a**) and SENT-"1231" (**b**) specimens with deep crack together with the crack propagation paths of SENT-"121" (**c**) and SENT-"1231" (**d**) specimens with deep crack.

3.3. CCT Specimen

3.3.1. Two Kinds of CCT Specimens with Shallow Crack

Figure 9 presents the fracture resistance curves and crack propagation paths of the CCT-"121" and CCT-"1231" specimens with shallow crack under different material constraints. Figure 9(a) and (b) presents that the fracture resistance curves of the CCT-"121" specimen and CCT-"1231" specimen show the similar trends. In addition, the fracture resistance curves of the CCT-"121" or CCT-"1231" specimens under different material constraints are similar except when the widths of material 52 Mb and material 52 Mw are 0 mm. It may be caused by the low geometry constraints of the CCT-"121" and CCT-"1231" specimens with shallow crack. Compared with SENB, CT, SENT, and CCT specimens, the CCT specimen has the lowest constraint. Under the low geometry constraint, the fracture resistance curve is insensitive to the changing of material constraint. In addition, because the fracture resistance curves are similar, only from the Figure 9, it is difficult to judge whether the fracture resistance curves reach a steady state or not, and whether an effect range of material constraint exists or not for the CCT specimen.

Figure 9(c) and (d) presents the crack propagation paths of the CCT-"121" and "1231" specimens with shallow crack. Figure 9(c) presents that all the cracks propagate straight and have not changed considerably under different material constraints in the CCT-"121" specimens with shallow crack. It is because that the initial crack is located in the center of the material 52 Mb, the strengths of materials at both sides of the crack are symmetric. In the Figure 9(d), the crack propagation paths also have not changed considerably under different material constraints. Different from the Figure 9(c), it is caused by the low geometry constraint in the CCT-"1231" specimen with shallow crack. Under the low geometry constraint, the crack propagation path is insensitive to the changing of the material constraint.

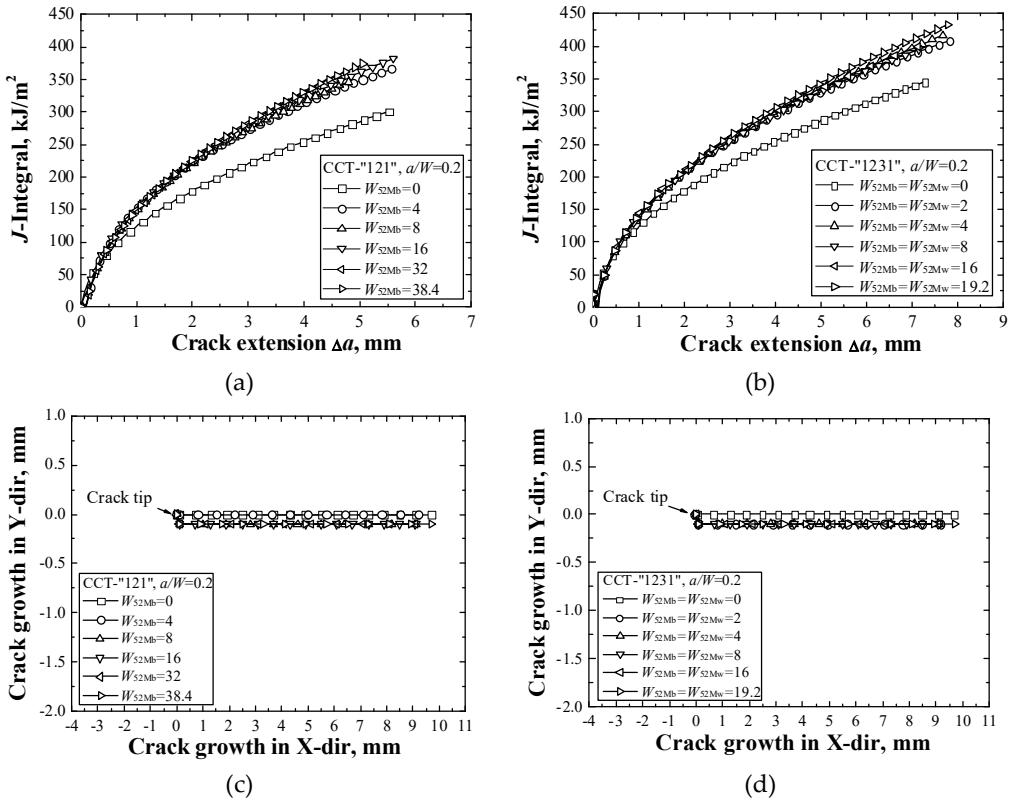

Figure 9. The fracture resistance curves of CCT-"121" (**a**) and CCT-"1231" (**b**) specimens with shallow crack together with the crack propagation paths of CCT-"121" (**c**) and CCT-"1231" (**d**) specimens with shallow crack.

3.3.2. Two Kinds of CCT Specimens with Deep Crack

Figure 10 presents the fracture resistance curves and crack propagation paths of the CCT-"121" and CCT-"1231" specimens with deep crack under different material constraints.

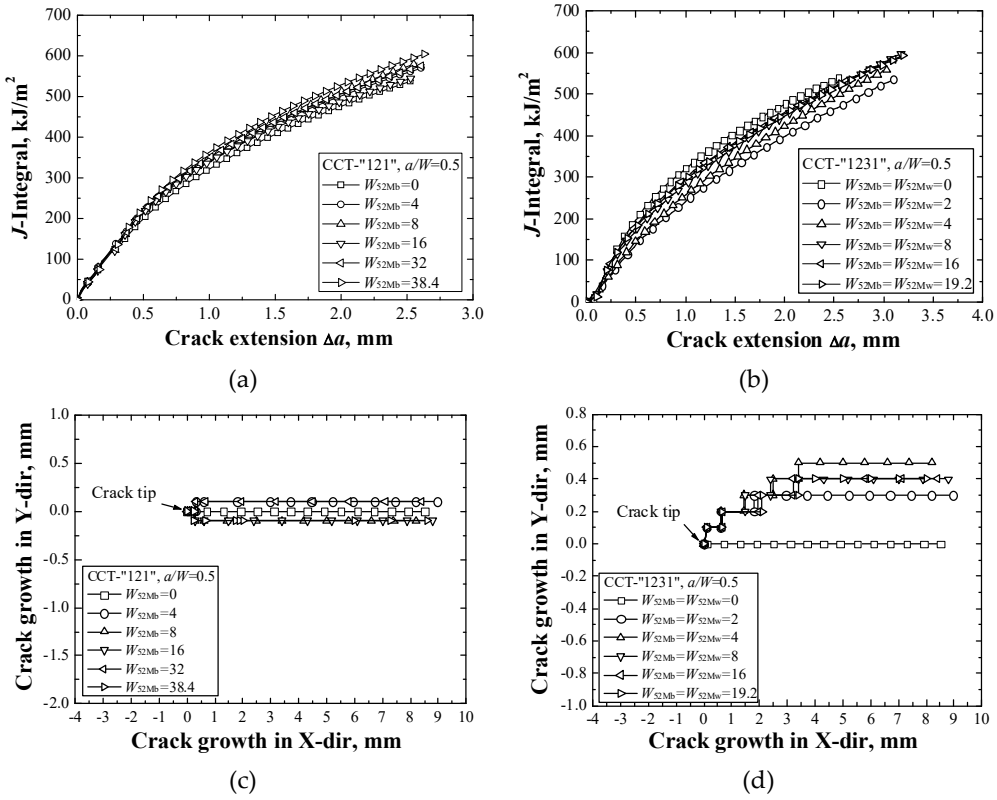

Figure 10. The fracture resistance curves of CCT-"121" (**a**) and CCT-"1231" (**b**) specimens with deep crack together with the crack propagation paths of CCT-"121" (**c**) and CCT-"1231" (**d**) specimens with deep crack.

Figure 10 (a) presents the fracture resistance curves of the CCT-"121" specimens with deep crack. Similarly with the CT-"121" and SENT-"121" specimens, it is also related to the strengths of the materials A508 and 52Mb. Because the strength of the material 52 Mb is higher than the material A508, the increasing of the width of material 52 Mb increases the fracture resistance of the specimen.

Different from the Figure 10 (a), Figure 10 (b) presents that the fracture resistance curves of the CCT-"1231" specimens with deep crack decrease first then increase, and finally remain steady with increasing of the widths of material 52 Mb and material 52 Mw. Similarly, with the CT-"1231" and SENT- "1231" specimens with deep crack in the Figures 6 (b) and 8 (b), the decreasing of the fracture resistance curves is also related to the high geometry and material constraints of the CCT-"1231" specimen with deep crack. The high constraints decrease the fracture resistance curve first. When the widths of material 52 Mb and material 52 Mw reach 8 mm, the total width of them exceeds the effect range of material constraint, and the fracture resistance curves of the CCT-"1231" specimens with deep crack no longer change. Because the material constraint of the CCT-"121" specimen is lower than CCT-"1231" specimen, the fracture resistance curves of the CCT-"121" specimens in the Figure 10(a) have not decreased.

Figure 10 (c) presents that all the cracks propagate straight and have not changed considerably under different material constraints in the CCT-"121" specimens with deep crack. Similarly, with the other "121" specimens, it is also because that the strengths of materials at the both sides of the crack are symmetric.

For the CCT-"1231" specimen with deep crack in the Figure 10 (d), it can be found that the crack propagation paths deviate to the side of material 52Mb which has a higher strength than material 52Mw in the process of crack growth. Similarly with SENT-"1231" specimen with deep crack in the

Figure 8 (d), it may be related to the loading configuration. The crack propagation path deviates to the side of high strength under the shearing stress in the CCT specimen.

Considering both Figures 9 and 10, we can arrive to a conclusion that the effect range of material constraint also exists in the CCT specimen.

3.4. The Contrast of Different Laboratory Specimens

Compared with the results of the SENB specimen in the previous studies [24,25] and the CT, SENT, and CCT specimens in this study, it can be found that the effect range of material constraint exists in all the specimens with different specimen geometries and loading configurations. Because these specimens are universal, we can arrive to a conclusion that the effect range of material constraint exists in all the strength mismatched specimens and structures. When a material located outside the effect range of material constraint, the fracture resistance curves, and crack propagation paths of the specimens and structures are no longer influenced by the mechanical properties of the material.

In addition, the numerical value of the effect range is affected by the geometry constraint. The specimen with deep crack (high geometry constraint) has smaller effect range than the specimen with shallow crack (low geometry constraint); the SENB and CT specimens (high geometry constraint specimens) have smaller effect range than the SENT and CCT specimens (low geometry constraint specimens).

Furthermore, different from the other specimens, for the specimens with high geometry and material constraints (CT-"121" specimen with deep crack, CT-"1231" specimen with deep crack, SENT-"1231" specimen with deep crack, CCT-"1231" specimen with deep crack), the fracture resistance curves decrease first with the changing of material constraint. The high geometry constraint and material constraint decrease the fracture resistance curve first.

There are also some differences between different laboratory specimens in the crack propagation path. For all the "121" specimens with center crack, the cracks propagate straight and have not changed considerably under different material constraints. For the "1231" specimens with interface crack, the crack propagation path deviates to the side of material that has a lower strength in the process of crack growth under bending stress (CT-"1231" specimen with shallow crack, CT-"1231" specimen with deep crack). The crack propagation path deviates to the side of the material that has a higher strength in the process of crack growth under shearing stress (SENT-"1231" specimen with deep crack, CCT-"1231" specimen with deep crack). For the "1231" specimens with low geometry constraint (SENT-"1231" specimen with shallow crack, CCT-"1231" specimen with shallow crack), the crack propagation paths are insensitive to the changing of material constraint.

In the future, the correlation of the effect range of material constraint with geometry constraint and strength mismatch should be established, and the effect range of material constraint of a structure can be obtained directly rather than by FEM simulations or experiments. Then, the results can provide scientific support for the structure integrity assessment and the design of strength mismatched structures.

4. Conclusions

In this study, different strength mismatched laboratory specimens that contain the CT, SENT, and CCT specimens with various specimen geometries, loading configurations, and initial cracks, and the effect range of the material constraint was systematically studied.

(1) Irrespective of the geometries and loading configurations, the center crack or interface crack, the shallow crack or deep crack, the effect range of material constraint exists in all the strength mismatched specimens and structures.

(2) The numerical value of the effect range is influenced by the geometry constraint. The high geometry constraint against the plastic deformation at crack tip reduces the effect range of material constraint. The specimen with deep crack has smaller effect range of material constraint than the specimen with shallow crack; the SENB and CT specimens have smaller effect ranges of material constraint than the SENT and CCT specimens.

(3) When a material is located outside the effect range of material constraint, the fracture resistance curves, and crack propagation paths of the specimens and structures are no longer influenced by the mechanical properties of the material.

(4) There exists an interaction between geometry constraint and material constraint. The high geometry constraints in the CT and SENB specimens strengthen the effect of material constraint. Under the low geometry constraint, the fracture resistance curve and crack propagation path are insensitive to the material constraint.

Author Contributions: Conceptualization, J. Y.; methodology, J. Y.; software, Y. D.; validation, Y. D., J. Y., and H.F. C.; writing—original draft preparation, Y. D.; writing—review and editing, J. Y. and H.F. C, All authors have read and agreed to the published version of the manuscript.

Funding: This research was funded by [National Natural Science Foundation of China] grant number [51975378].

Conflicts of Interest: The authors declare no conflict of interest.

References

1. Joch, J.; Ainsworth, R.A.; Hyde, T.H. Limit load and *J*-estimates for idealised problems of deeply cracked welded joints in plane-strain bending and tension. *Fatigue Fract. Eng. Mater. Struct.* **1993**, *16*, 1061–1079.
2. Burstow, M.C.; Ainsworth, R.A. Comparison of analytical, numerical and experimental solutions to problems of deeply cracked welded joints in bending. *Fatigue Fract. Eng. Mater. Struct.* **1995**, *18*, 221–234.
3. Zhang, Z.L.; Hauge, M.; Thaulow, C. Two-parameter characterization of the near-tip stress fields for a bi-material elastic-plastic interface crack. *Int. J. Fract.* **1996**, *79*, 65–83.
4. Betegón, C.; Peñuelas, I. A constraint based parameter for quantifying the crack tip stress fields in welded joints. *Eng. Fract. Mech.* **2006**, *73*, 1865–1877.
5. Yang, J.; Wang, G.Z.; Xuan, F.Z.; S. T., T.U. Unified characterisation of in-plane and out-of-plane constraint based on crack-tip equivalent plastic strain. *Fatigue Fract. Eng. Mater. Struct.* **2013**, *36*, 504–514.
6. Yang, J.; Wang, G.Z.; Xuan, F.Z.; Tu, S.T. Unified correlation of in-plane and out-of-plane constraints with fracture toughness. *Fatigue Fract. Eng. Mater. Struct.* **2014**, *37*, 132–145.
7. Yang, J.; Wang, G.Z.; Xuan, F.Z.; Tu, S.T. Unified correlation of in-plane and out-of-plane constraint with fracture resistance of a dissimilar metal welded joint. *Eng. Fract. Mech.* **2014**, *115*, 296–307.
8. Wang, H.T.; Wang, G.Z.; Xuan, F.Z.; Liu, C.J.; Tu, S.T. Local mechanical properties of a dissimilar metal welded joint in nuclear power systems. *Mater. Sci. Eng. A-Stract.* **2013**, *568*, 108–117.
9. Wang, H.T.; Wang, G.Z.; Xuan, F.Z.; Tu, S.T. An experimental investigation of local fracture resistance and crack growth paths in a dissimilar metal welded joint. *Mater. Des.* **2013**, *44*, 179–189.
10. Sarikka, T.; Ahonen, M.; Mouginot, R.; Nevasmaa, P.; Karjalainen-Roikonen, P.; Ehrnstén, U.; Hänninen, H. Effect of mechanical mismatch on fracture mechanical behavior of SA508 e Alloy 52 narrow gap dissimilar metal weld. *Int. J. Pres. Ves. Pip.* **2017**, *157*, 30–42.
11. Fan, K.; Wang, G.Z.; Tu, S.T.; Xuan, F.Z. Geometry and material constraint effects on fracture resistance behavior of bi-material interfaces. *Int. J. Fract.* **2016**, *201*, 143–155.
12. Fan, K.; Wang, G.Z.; Xuan, F.Z.; Tu, S.T. Effects of work hardening mismatch on fracture resistance behavior of bi-material interface regions. *Mater. Des.* **2015**, *68*, 186–194.
13. Fan, K.; Wang, G.Z.; Xuan, F.Z.; Tu, S.T. Local fracture resistance behavior of interface regions in a dissimilar metal welded joint. *Eng. Fract. Mech.* **2015**, *136*, 279–291.
14. Samal, M.K.; Balani, K.; Seidenfuss, M.; Roos, E. An experimental and numerical investigation of fracture resistance behaviour of a dissimilar metal welded joint. *Proc. Inst. Mech. Eng. Part C-J. Mech. Eng. Sci.* **2009**, *223*, 1507–1523.
15. Yang, F.Q.; Xue, H.; Zhao, L.Y.; Fang, X.R. Effects of Welded Mechanical Heterogeneity on Interface Crack Propagation in Dissimilar Weld Joints. *Adv. Mater. Sci. Eng.* **2019**, *2019*, 6593982.
16. Lindqvist, S.; Sarikka, T.; Ahonen, M.; Hänninen, H. The effect of crack path on tearing resistance of a narrow-gap Alloy 52 dissimilar metal weld. *Eng. Fract. Mech.* **2018**, *201*, 130–143.
17. Jang, C.; Lee, J.; Kim, J.S.; Jin, T.E. Mechanical property variation within inconel 82/182 dissimilar metal weld between low alloy steel and 316 stainless steel. *Int. J. Pres. Ves. Pip.* **2008**, *85*, 635–646.

18. Xue, H.; Sun, J. Study on micro region of crack tip of welded joints under different matches of yield stress. *Hot Work. Technol.* **2016**, *45*, 239–245.
19. Zhu, Z.Q.; Jing, H.Y.; Ge, J.G.; Chen, L.G. Effects of strength mis-matching on the fracture behavior of nuclear pressure steel A508-III welded joint. *Mater. Sci. Eng. A-Struct.* **2005**, *390*, 113–117.
20. Younise, B.; Rakinb, M.; Gubeljakc, N.; Medjob, B.; Sedmakd, A. Effect of material heterogeneity and constraint conditions on ductile fracture resistance of welded joint zones-Micromechanical assessment. *Eng. Fail. Anal.* **2017**, *82*, 435–445.
21. Xue, H.; Ogawa, K.; Shoji, T. Effect of welded mechanical heterogeneity on local stress and strain ahead of stationary and growing crack tips. *Nucl. Eng. Des.* **2009**, *239*, 628–640.
22. Khan, I.A.; Bhasin, V.; Chattopadhyay, J.; Ghosh, A.K. An insight of the structure of stress fields for stationary crack in strength mismatch weld under plane strain mode-I loading—Part I: Pure bending specimen. *Int. J. Mech. Sci.* **2012**, *62*, 89–102.
23. Khan, I.A.; Bhasin, V.; Chattopadhyay, J.; Ghosh, A.K. An insight of the structure of stress fields for stationary crack in strength mismatch weld under plane strain mode-I loading—Part II: Compact tension and middle tension specimens. *Int. J. Mech. Sci.* **2014**, *87*, 281–296.
24. Yang, J.; Wang, L. Effect range of the material constraint-I. Center crack. *Materials* **2019**, *12*, 67.
25. Dai, Y.; Yang, J.; Wang, L. Effect range of the material constraint-II. Interface crack. *Metals* **2019**, *9*, 696.
26. Yang, J.; Wang, L. Effect and optimal design of the material constraint in the DMWJ of nuclear power plants. *Acta Metall. Sin.* **2020**, in press.
27. Yang, J. Micromechanical analysis of in-plane constraint effect on the local fracture behavior of cracks in the weakest locations of dissimilar metal welded joint. *Acta Metall. Sin-Engl.* **2017**, *30*, 840–850.
28. Østby, E.; Thaulow, C.; Zhang, Z.L. Numerical simulations of specimen size and mismatch effects in ductile crack growth-Part I: Tearing resistance and crack growth paths. *Eng. Fract. Mech.* **2007**, *74*, 1770–1792.